IEEE Access
Multidisciplinary ⋮ Rapid Review ⋮ Open Access Journal

Received October 8, 2020, accepted October 15, 2020, date of publication October 26, 2020, date of current version November 10, 2020.

Digital Object Identifier 10.1109/ACCESS.2020.3033799

Robust Finite-Time Convergence Control Mechanism for High-Precision Tracking in a Hybrid Fluid Power Actuator

QUOC-DONG HOANG[1,2], VINICIO ALEJANDRO ROSAS-CERVANTES[1], SOON-GEUL LEE[1], IHN-SIK WEON[3], JAE-HWAN CHOI[1], AND YOUNG-HA KWON[1]

[1]Department of Mechanical Engineering, Kyung Hee University, Yongin 17104, South Korea
[2]Institute of Mechanical Engineering, Vietnam Maritime University, Hai Phong 182582, Vietnam
[3]Airport Industry Technology Research Institute, Incheon International Airport Corporation (IIAC), Incheon 22382, South Korea

Corresponding author: Soon-Geul Lee (sglee@khu.ac.kr)

This work was supported in part by the National Research Foundation of Korea, funded by the Ministry of Education under Grant 2019R1A2C2010195, in part by the Ministry of Science and Information & Communication Technology, South Korea, under the Grand Information Technology Research Center support program, supervised by the Institute for Information and Communications Technology Promotion (IITP) under Grant IITP-2019-2015-0-00742, in part by the Ministry of Trade, Industry, and Energy through the Robot Industrial Core Technology Development Project, supervised by Korea Evaluation Institute of Industrial Technology under Grant K_G012000921401, and in part by the Vietnam Maritime University.

ABSTRACT In this study, a novel multiphase converged control structure with a switching mechanism is established based on the fundamentals of the fast-terminal sliding mode. This control structure achieves an excellent performance in a nonlinear dynamic system, and its primary objective is to control the piston trajectory in an innovative electrohydraulic, pneumatic, and mechanical hybrid system. This work focuses on abrupt gain-scheduled acceleration, which has been rarely studied in the literature but has increasingly diverse high-technology applications across various industries. The greatest challenge lies in the sensitivity and instability of the system during a sudden actuator acceleration. Moreover, the system parameter uncertainties and external disturbances strongly influence the degree of control of the system. By inheriting the robustness and fast convergence properties of sliding-mode algorithms, the proposed control law not only guarantees a finite-time convergence of tracking errors to their origin but also reduces the impact of composite disturbances in an extremely rapid experimental process. The effectiveness of the proposed structure is analyzed via numerical simulations and industrial implementation.

INDEX TERMS Finite-time convergence, finite-time stability, robust sliding-mode control, acceleration tracking control, hydraulic actuator, pneumatic system.

I. INTRODUCTION

High-precision gain-scheduled acceleration is used by various industries in crash simulations [1], safety tests [2], absorbance system design [3], deconstruction machines, and dummy tests [4]. Fluid power control, which uses electrohydraulic system [5] and pneumatic control technologies [6], has attracted the attention of academics and industrial practitioners for many decades. Rapidly decelerating an actuator has a great impact on the external mass and internal reaction force inside the system. These working conditions require a platform that can absorb the reaction force of external loads while maintaining high energy output and precision. For this platform, a hybrid electro-hydraulic and pneumatic actuator (HEHPA) is designed as an innovative combination of hydraulic and pneumatic technologies. A pneumatic actuator with high-pressure gas can produce high energy output while simultaneously absorbing a high-level reaction force due to gas elasticity. The piston movement accuracy, which is the main weakness of pneumatic technology, can be guaranteed by using a hydraulic brake with a proper controller.

Control performance is influenced by the uncertainties and inaccuracies in modeling system dynamics and measuring parameters. A complex system that faces external disturbances has highly nonlinear properties and sensitivity in transition mode. For example, the variation in fluid viscosity

The associate editor coordinating the review of this manuscript and approving it for publication was Jinquan Xu.

affects the efficiency and flow of the fluid, changes the speed and pressure inside the brake chamber, and subsequently alters the friction control force and piston acceleration. Similarly, fluctuations in temperature and an increase in abrasion between piston and brake-pad surfaces significantly alter the friction coefficient, thereby changing the control force and movement of the actuator. Moreover, the actuator acceleration must be controlled within an short period. A strong convergence and robust control law are then necessary for handling these uncertainties, nonlinearities, and disturbances and for improving control quality.

Conventional sliding-mode controls (SMCs) [7]–[10], integral SMC (ISMC) [11]–[13], and super-twisting SMC (STSMC) [14] have been studied for more than a half of century due to their robust nature [15], [16] and short finite-time convergence [17]–[19]. These features are further enhanced in the fast-terminal version (FTSMC) [20]–[25]. Specifically, a nonlinear switching manifold substituting for a conventional sliding surface can substantially improve transient performance and shorten the convergence period [24], [25]. Therefore, FTSMC has been employed for a wide range of second-order nonlinear systems [26], [27], including under-actuated systems [20]. For a system with many uncertainties, the robustness of the controller [28] is essential. Meanwhile, this robust property is an inherent characteristic of sliding mode algorithms and FTSMC [29] that can be simply reinforced by combining with the adaptive law, such as observers [21]–[23]. These characteristics are potentially suitable for overcoming the aforementioned control problems.

In a control strategy with a dynamic system (1), (5-9), an input command signal (voltage) is sent to the servo valve to control the spool movement. Spool displacement determines the level of hydraulic pressure inside a brake chamber and controls the movement of a pneumatic piston. Detailed analyses are presented in Section 3. No direct relationship is observed between voltage and actuator acceleration given the nonlinear features of subsystems. A single controller developed based on mathematical dynamics also has limited applications. Moreover, the switch part of the dynamic model [30], [31], which is derived from the unbalanced properties of the servo valve circuit (8), (9), is included in the system. Based on the approaches described in [32], [33], this system can be described as a slow switching system. The greatest challenge in tracking rapidly changing acceleration lies in the highly nonlinear system and its extremely sensitive features. For example, a considerable variation in fluid viscosity is usually accompanied by changes in friction coefficients, asperity contacts, and fluctuations in oil temperature. The robust characteristics and ability of the switched law to reduce convergence time are therefore required in designing controllers. These problems both challenge and motivate us to build a control structure for achieving high-performance control.

The fundamental contributions of this work are given as follows.

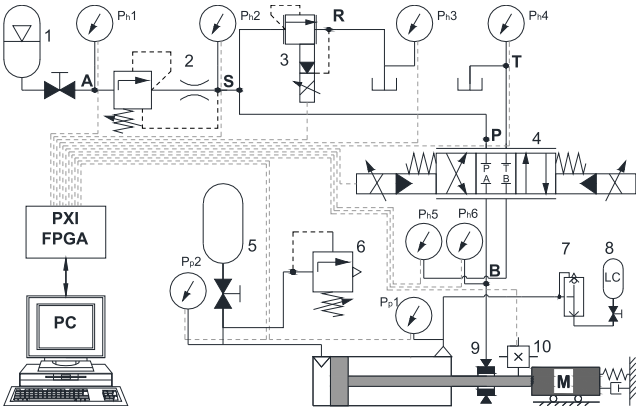

FIGURE 1. Experimental HEHPA system configuration: (1) Hydraulic bladder accumulator, (2) variable flow controller, (3) proportional pressure control valve, (4) proportional directional valve, (5) high-pressure supply unit, (6) relief valve, (7) quick exhaust valve, (8) low-pressure compressor, (9) hydraulic brake system, and (10) accelerometer, velocity, and displacement sensors.

i) This work presents a rare control problem (rapid acceleration tracking control in 0.1 s) and proposes a hybrid of pneumatic and hydraulic systems and its corresponding mathematical model that can achieve the required control quality. The physical characteristics of hydraulic fluid flows, directional valves, and mechanical brake–actuator system, which allow the application of nonlinear control, are described via dynamic equations.

ii) Comprehensive controllers for single first- and second-order nonlinear subsystems are developed. These controllers have enough robustness to overcome the effects of bounded uncertainties and disturbances.

iii) An alternative multistage sliding-mode control structure with switching mechanisms for the unbalanced dynamic part is developed. The finite-time stability and accuracy of the controlled system satisfy the work requirements and are analyzed via a simulation and experiment.

II. HEHPA AND EMPIRICAL DYNAMIC MODELING

A. HEHPA SYSTEM

Fig. 1 presents the detailed schematic of the industrial HEHPA system. The major mechanical element of this system is a pneumatic cylinder fixed with an external mass (M) and a hydraulic brake (9). The energy supplied for the positive movement of the actuator is derived from the pneumatic system. The compressed gas inside the high-pressure supply unit (5) maintains a roughly invariant pressure if the volume of the piston chamber and gas leakage are negligible. The alternative incompressible hydraulic pressure controls the presiding friction force and piston movement with an external load. An industrial desktop computer controls the entire system in real time through a reliable microcontroller-based field-programmable gate array. The physical system has three major subsystems, namely, a mechanical brake actuator, servo-hydraulics system, and pneumatic system.

Before reaching the waiting port (P) of the directional servo valve (4), the supply pressure is controlled by a proportional pressure control valve (3) to ensure a stable input pressure and an offset level that exceeds the desired hydraulic pressure inside the brake chamber, thereby enhancing control quality especially in cases with high-peak reference acceleration.

B. SYSTEM MODELING

Mathematical formulas highlight the dynamic behavior of the overall system in the transient working mode. Based on Newton's second law, the translational dynamics of a piston are defined as follows according to [34]–[36]:

$$\begin{aligned}&(m_P+m_L)\ddot{\chi}_P+b_P\dot{\chi}_P+K_L\chi_P\\&\quad+sgn(\dot{\chi}_P)\left(F_{fc0}+F_{fs0}e^{-|\dot{\chi}_P|c_s^{-1}}\right)+\Phi_D\\&\quad=-(a_P-a_R)p_{p1}-\mu_{d0}(n_ve^{-m_v\dot{\chi}_P}+1)a_Bp_B+a_Pp_{P2},\end{aligned}\tag{1}$$

where m_L and m_P are the masses of the external load and piston, respectively, b_P is the friction coefficient among the piston, the inner working surface of the cylinder, and the external damper, K_L is the equivalent stiffness applied on the hydraulic system, F_{fc0} and F_{fs0} are the Coulomb and static friction, respectively, a_R and a_P denote the cross-sectional areas of the piston rod and the effective piston-cylinder area, respectively, p_B denotes the hydraulic brake pressure, a_B denotes the brake pad effective area, μ_{d0} is the steady-state coefficient of friction between the piston rod and brake pad, m_v and n_v represent the parametric coefficient of the exponential friction-speed function and the multiplication factor, respectively, and $\Phi_D(t)$ is the bounded composite disturbance on the actuator movement.

The function $sgn(\dot{\chi}_P)\left(F_{fc0}+F_{fs0}e^{e^{-|\dot{\chi}_P|c_s^{-1}}}\right)$ expresses the external frictional force, which depends on the direction of the piston velocity vector as described by the sign of the actuator velocity $\dot{\chi}_P(t)$:

$$\mathrm{sgn}(\dot{\chi}_P)=\begin{cases}\dot{\chi}_P/|\dot{\chi}_P| & \dot{\chi}_P\neq 0\\ 0 & \dot{\chi}_P=0.\end{cases}\tag{2}$$

Based on actual working conditions, the composite disturbance in (1) is mainly caused by the vibration of the piston rod and the parameter estimation inaccuracy resulting from unpredictable variations and external disturbances. In a system where large state changes occur within a short period, relatively large variations can be observed in the parameters due to brake-pad imbalance and inaccuracies during manufacturing and assembly. The vibrations caused by external masses lead to system uncertainties that involve additional forces, $\Phi_D(t)$, directly affecting the system. Drawing on [37], overall disturbance can be modeled as a linear dynamic system of unmeasurable, time-varying, bounded disturbance functions. Given that neither these functions nor the initial conditions are measurable and only the ranges over which these functions can vary are known, one can describe the total composite disturbance as a time-varying bounded function $|\Phi_D(t)|\leq\breve{\Phi}_D(t)$.

The supply pressure at the input port of the directional valve depends on the flow through a P point and the flow that returns to the tank through the pressure control valve. Following [34], [36], [38], the supply pressure can be calculated as

$$\begin{aligned}\frac{V_S}{\beta_E}\dot{p}_S=&+C_{d1}A_F\sqrt{2(p_{h1}-p_S)\rho_H^{-1}}\\&-sgn(p_P-p_B)C_{d3}\pi D_{SV}sn(\chi_{SV})\\&\times\sqrt{2\rho_H^{-1}\left|(1-\eta_H)p_S-p_B\right|}\\&-C_{d2}\pi D_{pc}sn(-\chi_{PC})\sqrt{(p_S-p_{h3})\rho_H^{-1}},\end{aligned}\tag{3}$$

where C_{d1} is the discharge coefficient of the flow controller, A_F is the total flow area, ρ_H is the hydraulic fluid density (a function of Reynolds and cavitation numbers), $sn(\chi)$ is a rectifier linear unit of χ, and C_{d2} and C_{d3} are the discharge coefficients of the pressure control and directional servo valves, respectively. The variables $\omega_{pc}=\pi D_{pc}$ and $\omega_{SV}=\pi D_{SV}$ are the perimeters of the slide valve orifices, with D_{SV} and D_{PC} representing the base diameters of the spools of the hydraulic servo valves. As functions of input signals u_{PC} and u_S, $\chi_{pc}(t)$ and $\chi_{sv}(t)$ represent the positions of spool servo valves, β_E is the hydraulic effective bulk modulus, and V_B is the brake chamber volume.

In case of turbulent flow, when pressurized fluid is transmitted in the pipe, the influence of viscous friction is determined by $\eta_H=1.79\mu^{0.25}\rho_H^{0.75}Q_F^{1.75}l_{p1}\pi^{-1.75}p_S^{-1}d_p^{-4.57}$ in (3). Here, $Q_F(t)$ is the flow at the flow controller, μ is the hydraulic fluid dynamic viscosity, l_{p1} is the pipe length from S to the directional servo valve, and d_p is the inner diameter of the hydraulic pipe.

The spool displacement of the pressure control valve, $\chi_{PC}(t)$, is formulated as follows following [34], [36], [38]:

$$\begin{aligned}&m_{PC}\ddot{\chi}_{PC}+b_{PC}\dot{\chi}_{PC}+c_{PC}\chi_{PC}+0.25\pi C_fD_{PC}^2(p_{h3}-p_S)\\&\qquad=-m_{PC}K_{PC}u_{PC},\end{aligned}\tag{4}$$

where m_{PC} denotes the spool mass, b_{PC} and c_{PC} are the damping coefficients when the spool moves and the equivalent stiffness of the servo valve's return springs, respectively, K_{PC} is the input gain of the controller, u_{PC} is the input voltage to the valve, and C_f indicates the fluid-force coefficient caused by the difference between the inside pressure p_S and outside pressure p_{h3}.

The dynamic behavior of pressure in the brake chamber [34], [36], [38] can be calculated as

$$\begin{aligned}\frac{V_B}{\beta_E}\dot{p}_B=&\,sgn(p_P-p_B)C_{d3}\pi sn(\chi_{SV})D_{SV}\\&\times\sqrt{2\rho_H^{-1}\left|(1-\eta_H)p_S-p_B\right|}\\&-C_{d4}\pi sn(-\chi_{SV})D_{SV}\sqrt{2(p_B-p_T)\rho_H^{-1}},\end{aligned}\tag{5}$$

where C_{d4} is the discharge coefficient of the proportional directional servo valve in the case of A–T connection.

The position of the hydraulic directional servo valve spool, $\chi_{SV}(t)$, is formulated as follows according to [34], [36], [38]:

$$\ddot{\chi}_{SV}\omega_{SV}^{-2} + 2\xi_{SV}\omega_{SV}^{-1}\dot{\chi}_{SV} + \chi_{SV} + F_f = K_U u_S, \quad (6)$$

where ω_{SV} and ξ_{SV} are the natural frequency of the servo valve and the damping ratio, respectively, and F_f denotes the steady flow force, which is calculated as follows according to [36]:

$$F_f = 2\lambda_1 \Delta p C_{d3}^2 A_o \cos(\theta_v), \quad (7)$$

where Δp is the pressure drop level, θ_v is the jet angle, $\lambda_1$is the adjustment coefficient, and A_0 is the function of the opened area of the outlet port, which is calculated as $2D_S\chi_{SV}\sin^{-1}(H_S/D_S)$, where D_S and H_S represent the spool diameter of the servo valve and the outlet port height, respectively.

The requirements of varied pressure inside the brake chamber lead to an imbalance in designing the directional servo valve. According to (5), an increase in hydraulic pressure in the entire brake chamber coincides with the connection of ports P and B in the proportional directional valve. In case A, the brake pressure surge over time can be computed as

$$\frac{V_B}{\beta_E}\dot{p}_B = sgn(p_P - p_B)C_{d3}\pi D_{SV}\,|\chi_{SV}| \times \sqrt{2\rho_H^{-1}\,|(1-\eta_H)\,p_S - p_B|}. \quad (8)$$

Meanwhile, in case B,

$$\dot{p}_B = -C_{d4}\pi D_{SV}\,|\chi_{SV}|\,\beta_E V_B^{-1}\sqrt{2(p_B - p_T)\rho_H^{-1}}. \quad (9)$$

When the supply pressure is set to

$$p_{ST} = \left(\frac{1}{\eta_H} + \frac{C_{d4}^2}{\eta_H C_{d3}^2}\right)\bar{p}_B, \quad (10)$$

the same amount of fluid flows through the valve in both directions. The imbalance can therefore be ignored. Here, $\bar{p}_B$ is the average value of brake pressure.

The system dynamics should be simplified to achieve rapid sampling times and high-speed control performance. To accelerate the computation and control processes, the following assumptions are made based on actual operating conditions and technical requirements:

Assumption 01: χ_{32} is always greater than 0 when $t > 0$, and $sgn(\dot{\chi}_P) = 1$.

Assumption 02: The average brake pressure is set to $\bar{p}_B \approx$ 45 bars, whereas the desired supply pressure p_{ST} is set to 100 bars. As a result, p_P is always greater than p_B, and $sgn(p_P - p_B) = 1$. Condition (10) is also satisfied.

III. ADVANCED CONTROL STRATEGY FOR SUDDEN GAIN-SCHEDULED ACCELERATION

A. COMPREHENSIVE SMCS FOR SISO SUBSYSTEMS

1) FTSMC FOR SECOND-ORDER SUBSYSTEMS

Second-order nonlinear SISO subsystems can be described as

$$\dot{\chi}_1 = \chi_2, \quad \dot{\chi}_2 = \varphi(\boldsymbol{\chi}_s, \boldsymbol{\chi}_p, t) + \theta(\boldsymbol{\chi}_s, \boldsymbol{\chi}_p, t)\tau(t) + \Phi_f(t), \quad (11)$$

where $\varphi(\boldsymbol{\chi}_s, \boldsymbol{\chi}_p, t)$ and $\theta(\boldsymbol{\chi}_s, \boldsymbol{\chi}_p, t) \neq 0$ are nonlinear dynamic functions, and $\tau(t)$ is the command input of the subsystem. $\Phi_f(t)$ is the function of composite disturbance whose first-time derivative constitutes time-varying bounded functions $\left(\left|\Phi_f(t)\right| \leq \breve{\Phi}_f\right)$ and $\left(\left|\dot{\Phi}_f(t)\right| \leq \breve{\Phi}_{fd}\right)$, $\boldsymbol{\chi}_s = [\chi_1, \chi_2]^T = [\chi, \dot{\chi}]^T$ is a vector of controlled subsystem states, and $\boldsymbol{\chi}_p = [\varsigma_1, \varsigma_2, \ldots, \varsigma_h, \ldots, \varsigma_m]^T$, $(h, m \in \mathbb{N})$, where ς_h denotes the real-time system parameters. The target trajectories of the states are $\boldsymbol{\chi}_{sT} = [\chi_{1T}, \chi_{2T}]^T = [\chi_T, \dot{\chi}_T]^T$, and the vector of the tracking error is $\tilde{\boldsymbol{\chi}}_s = \boldsymbol{\chi}_s - \boldsymbol{\chi}_{sT} = \left[\tilde{\chi}_1, \tilde{\chi}_2\right]^T = \left[\tilde{\chi}, \dot{\tilde{\chi}}\right]^T = \left[\tilde{\chi}_1 - \chi_T, \tilde{\chi}_2 - \dot{\chi}_T\right]^T$.

For the second-order subsystem (11), which is a finite-time stable control law, a fast-terminal sliding mode is applied with the following exponential sliding variable:

$$\zeta_f(t) = \beta_1\tilde{\chi}_1 + \beta_2\tilde{\chi}_1^{\frac{\alpha}{\gamma}} + \tilde{\chi}_2 = \beta_1\tilde{\chi} + \beta_2\,\mathrm{sgn}(\tilde{\chi})^{\frac{\alpha}{\gamma}} + \dot{\tilde{\chi}}, \quad (12)$$

or

$$\zeta_f(t) = \chi_2 - \chi_{2T} + \beta_1(\chi_1 - \chi_{1T}) + \beta_2\,\mathrm{sgn}(\chi_1 - \chi_{1T})^{\frac{\alpha}{\gamma}}, \quad (13)$$

where β_1 and β_2 are strictly positive parameters, and the positive integers α and γ satisfy $\alpha < \gamma < 2\alpha$. The function $\beta_2\,\mathrm{sgn}(\tilde{\chi})^{\frac{\alpha}{\gamma}}$ is then defined as

$$\beta_2\,\mathrm{sgn}(\tilde{\chi})^{\frac{\alpha}{\gamma}} \triangleq \mathrm{sgn}(\tilde{\chi})\,|\tilde{\chi}|^{\frac{\alpha}{\gamma}}, . \quad (14)$$

TSM function (6) is continuous and differentiable even though the absolute value and signum operators are involved. The first derivative of this function can be expressed as (see Appendix A), and the first-order derivative of (12) is computed as

$$\dot{\zeta}_f(t) = \dot{\chi}_2 - \dot{\chi}_{2T} + \beta_1(\dot{\chi}_1 - \dot{\chi}_{1T}) + \beta_2\alpha\gamma^{-1}(\dot{\chi}_1 - \dot{\chi}_{1T})\,|\chi_1 - \chi_{1T}|^{\frac{\alpha-\gamma}{\gamma}}, \quad (15)$$

This calculation is based on the following lemma:

Lemma 1: The FTSMC control law [39] for the given second-order subsystem (11) is comprehensively designed as

$$\tau(t) = \Delta_f \times \theta^{-1}(\boldsymbol{\chi}_s, \boldsymbol{\chi}_p, t), \quad (16)$$

with

$$\Delta_f = \Big\{-\mu_{f1}\zeta_f(t) - \beta_1(\dot{\chi}_1 - \dot{\chi}_{1T}) - \mu_{f2}\,\mathrm{sgn}\left(\zeta_f(t)\right)^{\varepsilon} + \dot{\chi}_{2T} - \varphi(\boldsymbol{\chi}_s, \boldsymbol{\chi}_p, t) - \mu_{f3}\,\mathrm{sgn}\left(\zeta_f(t)\right) - \beta_2\alpha\gamma^{-1}(\dot{\chi}_1 - \dot{\chi}_{1T})\,|\chi_1 - \chi_{1T}|^{\frac{\alpha}{\gamma}-1}\Big\}, \quad (17)$$

where μ_{f1}, μ_{f2}, and μ_{f3} are positive controller gains. This controller satisfies the sliding condition where $\varepsilon \in \Re$, $0 < \varepsilon < 1$, and $\mathrm{sgn}\left(\zeta_f(t)\right)^{\varepsilon}$ means $\mathrm{sgn}\left(\zeta_f(t)\right)\left|\zeta_f(t)\right|^{\varepsilon}$.

Proof: Consider the defined Lyapunov candidate function

$$\Upsilon_f(t) = \frac{1}{2}\left(\zeta_f^2(t)\right). \tag{18}$$

According to (11), (15), (16), and (17), differentiating (18) with respect to time yields

$$\begin{aligned}\dot{\Upsilon}_f(t) &= \frac{d\Upsilon_f}{d\zeta_f}\frac{d\zeta_f}{dt}\\ &= \zeta_f(t)\begin{Bmatrix}-\mu_{f1}\zeta_f(t) - \mu_{f2}\,\mathrm{sgn}\left(\zeta_f(t)\right)^{\varepsilon}\\ -\mu_{f3}\,\mathrm{sgn}\left(\zeta_f(t)\right) + \Phi_f(t)\end{Bmatrix}\\ &\le \begin{Bmatrix}-\mu_{f1}\left(\zeta_f(t)\right)^2 - \mu_{f2}\left|\zeta_f(t)\right|^{1+\varepsilon}\\ +\left|\zeta_f(t)\right|\breve{\Phi}_f(t) - \mu_{f3}\left|\zeta_f(t)\right|\end{Bmatrix}\\ &\Rightarrow \dot{\Upsilon}_f(t) \le \begin{Bmatrix}-\mu_{f1}\left(\zeta_f(t)\right)^2 - \mu_{f2}\left|\zeta_f(t)\right|^{1+\varepsilon}\\ -\left|\zeta_f(t)\right|\left(\mu_{f3} - \breve{\Phi}_f(t)\right)\end{Bmatrix}.\end{aligned} \tag{19}$$

The real function $\Upsilon_f(t)$ is always positive or equal to 0 $\left(\Upsilon_f(t) \ge 0,\ \zeta_f(t) \in \Re\right)$. If the selected controller gains satisfy $\mu_{f1} > 0$, then $\mu_{f2} > 0$, μ_{f3} is selected, and $\mu_{f3} = \mu_{f3}^*$is guaranteed. When $\mu_{f3} - \breve{\Phi}_f(t) \ge 0$, the derivative of the Lyapunov function (19) $\dot{\Upsilon}_f\left(\tilde{\chi}_s, t\right)$is always negative or equal to 0 $\left(\dot{\Upsilon}_f(t) \le 0\right)$. The function$\Upsilon_f(t) \le \Upsilon_f(0)$ decreases when $t \to \infty$. Function (18) is Lyapunov stable, and the sliding condition is guaranteed. The tracking errors converge to their origin, thereby ending the proof of Lemma 1.

Lemma 2: For a continuous dynamic system (32), the sliding surface (33) is asymptotically stable with the control law (35).

Proof: Set $\hat{\mu}_{f3} = \mu_{f3}^* - \breve{\Phi}_f$, then

$$\dot{\Upsilon}_f(t) \le \left\{-\mu_{f1}\left(\zeta_f(t)\right)^2 - \hat{\mu}_{f3}\left|\zeta_f(t)\right|\right\} \le 0. \tag{20}$$

Integrating this equation yields

$$\int_0^t \dot{\Upsilon}_f(t)dt \le \int_0^t \left\{-\mu_{f1}\left(\zeta_f(t)\right)^2 - \hat{\mu}_{f3}\left|\zeta_f(t)\right|\right\}dt. \tag{21}$$

One can then infer

$$\lim_{t\to\infty}\int_0^t \left\{+\mu_{f1}\left(\zeta_f(t)\right)^2 + \hat{\mu}_{f3}\left|\zeta_f(t)\right|\right\}dt < \infty, \tag{22}$$

and

$$\lim_{t\to\infty}\int_0^t \mu_{f1}\left(\zeta_f(t)\right)^2 dt < \infty, \quad \lim_{t\to\infty}\int_0^t \hat{\mu}_{f3}\left|\zeta_f(t)\right|dt < \infty. \tag{23}$$

Given that

$$\begin{aligned}\Upsilon_f(0) &\ge \Upsilon_f(t) + \int_0^t \left\{+\mu_{f1}\left(\zeta_f(t)\right)^2 + \hat{\mu}_{f3}\left|\zeta_f(t)\right|\right\}dt\\ &\ge \int_0^t \left\{+\mu_{f1}\left(\zeta_f(t)\right)^2 + \hat{\mu}_{f3}\left|\zeta_f(t)\right|\right\}dt,\end{aligned} \tag{24}$$

one can obtain $\zeta_f(t) \in L_1$ and $\zeta_f(t) \in L_2$.

Furthermore,

$$\begin{aligned}\Upsilon_f(t) &\le \Upsilon_f(0) - \int_0^t \left\{+\mu_{f1}\left(\zeta_f(t)\right)^2 + \hat{\mu}_{f3}\left|\zeta_f(t)\right|\right\}dt\\ &\le \Upsilon_f(0) \le \infty,\end{aligned} \tag{25}$$

and $\zeta_f(t) \in L_\infty$.

By contrast, if $\dot{\Upsilon}_f(t) = \dot{\zeta}_f(t)\,\zeta_f(t) \le 0$, then $\dot{\zeta}_f(t) \in L_\infty$.

According to the collected evidence, function $\zeta_f(t)$ is asymptotically stable. This function approaches 0 $\left(\zeta_f(t) \to 0\right)$ as time approaches infinity $(t \to \infty)$, that is, $\lim_{t\to\infty}\zeta_f(t) = 0$. The reaching time is $t_{fr} \le \left|\zeta_f(0)\right|\mu_f^{-1}$ according to [37], [40], [41], thereby ending the proof of Lemma 2.

Given that the control strategy primarily focuses on the piston movement with mass (1) and that the greatest control challenge is derived from this subsystem, a thorough investigation of the second-order fast-terminal sling mode for finite-time stability is necessary. The fundamental concepts of finite-time stability have been discussed in many reports, including those by Fridman [42]–[44]. One state-of-the-art perspective is described as follows:

Definition 1 [43], [44]: Consider a system

$$\dot{\chi} = f(\chi), \tag{26}$$

where $\chi \in \Re^n$. Afterward, $f(0) = 0$, and $f(\chi) : D \to \Re^n$ is continuous in the open neighborhood D of the origin. The equilibrium point $\chi = 0$ of the system is finite-time stable if this point is Lyapunov stable and finite-time convergent in neighborhood $U \subseteq D$. The term finite-time convergence indicates that for an arbitrary initial condition $\chi_0 \in U/\{0\}$, there is a settling time function $T(\chi_0) : U/\{0\} \to (0, \infty)$ such that every solution $\chi(t, \chi_0)$ of the system (26) is defined as $\chi(t, \chi_0) \in U/\{0\}$ for $t \in [0, T(\chi_0))$, thereby ensuring $\lim_{t\to T(\chi_0)}\chi(t, \chi_0) = 0$ and $\chi(t, \chi_0) = 0$ if $t \ge T(\chi_0)$.

Definition 2 [42]–[44]: Consider the non-autonomous system

$$\dot{\chi} = f(\chi) + g(\chi)u, \tag{27}$$

where $\chi \in \Re^n$ and $u \in \Re^m$. In this case, $f(0) = 0$, $g(\chi) \ne 0$, and $f(\chi) : D \to \Re^n$. The closed-loop system can be stabilized in finite time if there is a feedback control law $u$such that $\chi = 0$ represents the finite-time stable equilibrium of the given system.

Lemma 3: If the equilibrium point $\chi = 0$ of the continuous differential equation is globally finite-time stable for any given initial condition $\chi(0) = \chi_o$, then the tracking error $\tilde{\chi}_s$ converges to $\tilde{\chi}_s \equiv 0$ in finite time and remains 0 forever. Following [42], [43], [45], [46], if the non-negative Lyapunov function $L(\chi)$ satisfies the condition

$$\dot{L}(\chi) + \beta_l L^{\gamma_l}(\chi) \le 0, \tag{28}$$

where the coefficients are $\beta_l > 0$ and $0 < \gamma_l < 1$, then the system is finite-time stable. The convergence time is $t \leq 2\delta^{-1}L^{\frac{1}{2}}(0)$, where δ is the function of the controller parameters [42], [43], [47]–[49].

According to [42], [50], [51], an extended Lyapunov function that illustrates finite-time stability for a fast terminal sliding mode is defined as

$$\dot{L}(\chi) + \alpha_l L(\chi) + \beta_l L^{\gamma_l}(\chi) \leq 0, \tag{29}$$

where α_l, $\beta_l > 0$ and $0 < \gamma_l < 1$. The settling time is generally obtained by

$$T(\chi_0) \leq \frac{1}{\alpha_l(1-\gamma_l)} \ln\left(\frac{\alpha_l L^{1-\gamma_l}(\chi_0) + \beta_l}{\beta_l}\right). \tag{30}$$

Condition (29) is strong and ensures inequality (28) because $\alpha_l L(\chi)$ is non-negative.

The basis of Lemma 3 is proven by Fridman, Levant, and several other studies, such as [42], [43], [45], [46]. This lemma has also been successfully applied in numerous studies, such as in [45], [50], [52], [53].

According to (19), if $\mu_{f3} > \breve{\Phi}_f$, then one can infer

$$\dot{\Upsilon}_f(t) \leq -\mu_{f1}\left(\zeta_f(t)\right)^2 - \mu_{f2}\left|\zeta_f(t)\right|^{\varepsilon}\left|\zeta_f(t)\right|, . \tag{31}$$

Eventually, the function $\Upsilon_f(t)$ satisfies the conditions specified in Lemma 3. The investigated candidate function and second-order system are then finite-time stable with the control law shown in Lemma 1.

The settling time is given in Lemma 3 and can be directly calculated in Lemma 7.

2) ISMC FOR FIRST-ORDER SUBSYSTEMS

We consider the first-order nonlinear subsystem

$$\begin{aligned} \dot{\chi}_s &= \varphi(\chi_s, \boldsymbol{\chi}_p, t) + \theta(\chi_s, \boldsymbol{\chi}_p, t)\tau(t) + \Phi_i(t), \\ y &= \chi_s^{(k_0)} \quad (k_0 = \{0, 1\}), \end{aligned} \tag{32}$$

where $\varphi(\chi, \boldsymbol{\chi}_p, t)$ and $\theta(\chi, \boldsymbol{\chi}_p, t) \neq 0$ are dynamic nonlinear functions, $\Phi_i(t)$ is the bounded composite disturbance impacting the subsystem that satisfies $|\Phi_i(t)| \leq \breve{\Phi}_i$ and $\left|\dot{\Phi}_i(t)\right| \leq \breve{\Phi}_{id}$, and $\tau(t)$ is the input command signal. $\boldsymbol{\chi}_p = [\varsigma_1, \varsigma_2, \ldots, \varsigma_h, \ldots, \varsigma_m]^T$ and $(h, m \in \mathbb{N})$, where ς_h represents the time-varying parameters of the subsystem. Meanwhile, χ_s and χ_{sT} are state variable with the target value, and $\tilde{\chi}_s = \chi_s - \chi_{sT}$ is defined as the tracking error.

ISMC is a classical controller that has been widely used for many decades [41], [54]. The sliding variable of this controller is defined as

$$\zeta_i(t) = \beta_i \int_0^t \tilde{\chi}_s d\tau + \tilde{\chi}_s = \beta_i \int_0^t (\chi_s - \chi_{sT})\, d\tau + \chi_s - \chi_{sT}, \tag{33}$$

where β_i is the controller coefficient.

Accordingly,

$$\dot{\zeta}_i(t) = \beta_i \tilde{\chi}_s + \dot{\tilde{\chi}}_s = \beta_i(\chi_s - \chi_{sT}) + \dot{\chi}_s - \dot{\chi}_{sT}. \tag{34}$$

Lemma 4: For subsystem (32), the general finite-time-convergence ISMC law is formulated as

$$\tau(t) = \Delta_i \times \theta^{-1}(\chi_s, \boldsymbol{\chi}_p, t), \tag{35}$$

where

$$\Delta_i = \left\{ \begin{array}{l} -\mu_{i2}\,\mathrm{sgn}\left(\zeta_i(t)\right) + \dot{\chi}_{sT} - \beta_i(\chi_s - \chi_{sT}) \\ -\varphi(\chi_s, \boldsymbol{\chi}_p, t) - \mu_{i1}\left|\zeta_i(t)\right|^{\frac{1}{2}}\,\mathrm{sgn}\left(\zeta_i(t)\right) \end{array} \right\}, \tag{36}$$

which guarantees the sliding condition.

Proof: The Lyapunov candidate function is selected as

$$\Upsilon_i(t) = 0.5\left(\zeta_i^2(t)\right). \tag{37}$$

From (32), (34), (35), and (36), the first-order time derivative of function (37) can be calculated as

$$\dot{\Upsilon}_i(t) = \zeta_i(t)\left\{ \begin{array}{l} -\mu_{i1}\left|\zeta_i(t)\right|^{\frac{1}{2}}\,\mathrm{sgn}\left(\zeta_{i2}(t)\right) \\ -\mu_{i2}\,\mathrm{sgn}\left(\zeta_i(t)\right) + \Phi_i(t) \end{array} \right\}. \tag{38}$$

μ_{i2}^* guarantees $\mu_{i2}^* - \breve{\Phi}_{id} \geq 0$ when the value of μ_{i2} is $\mu_{i2} = \mu_{i2}^*$, and$\dot{\Upsilon}_i(t)$ is always negative or equal to 0 $\left(\dot{\Upsilon}_i(t) \leq 0\right)$ and $(\Upsilon_i(t) \geq 0)$ as$\zeta_i(t) \in \Re$. $t \to \infty$ yields $\Upsilon_i(t) \leq \Upsilon_i(0)$, thereby suggesting that $\zeta_i^2(t)$, $(\zeta_i(t) \in \Re)$ is decreasing. Consequently, the candidate function is stable in a Lyapunov sense. Furthermore, the sliding condition is guaranteed, and the tracking errors are consolidated to zero following the convergence of the sliding surface.

The fundamentals of the sliding-mode control law have been reported by Utkin in 1992 [37], [55] and by other authors [56], [57].

The proof of Lemma 4 is thus completed.

Lemma 5: The continuously nonlinear subsystem (32) is asymptotically stable for control laws (35) and (36).

Proof: Lemma 5 is proven in an approach similar to that used for Lemma 2.

Lemma 6: For dynamic system (32), the control law given in Lemma 4 ensures the finite-time stability of the closed-loop system with the convergence time satisfying $t_{ic} \leq 2\delta_i^{-1}\Upsilon_i^{\frac{1}{2}}(0)$. Here, δ_i is the function computed from the controller coefficients.

Proof: Form (38), if the value of μ_{i2} is $\mu_{i2} = \mu_{i2}^* \geq \breve{\Phi}_{id}$, then one can infer that $\left(\mu_{i2} - \breve{\Phi}_{id}(t)\right) \geq 0$. Consequently,

$$\dot{\Upsilon}_i(t) \leq -\mu_{i1}\left|\zeta_i(t)\right|^{\frac{1}{2}}\left|\zeta_i(t)\right|. \tag{39}$$

Following [29], the uniform Lyapunov function $\Upsilon_i(t)$ enters a ball with radius $\Upsilon_i(0)$ in finite time. Eventually, the given first-order system (32) with bounded composite function $\Phi_i(t)$ is inferred to be finite-time stable based on Lemma 3, hence ending the proof of Lemma 6.

This lemma has been proven and applied in recent works, including [34], [35], [47]–[50].

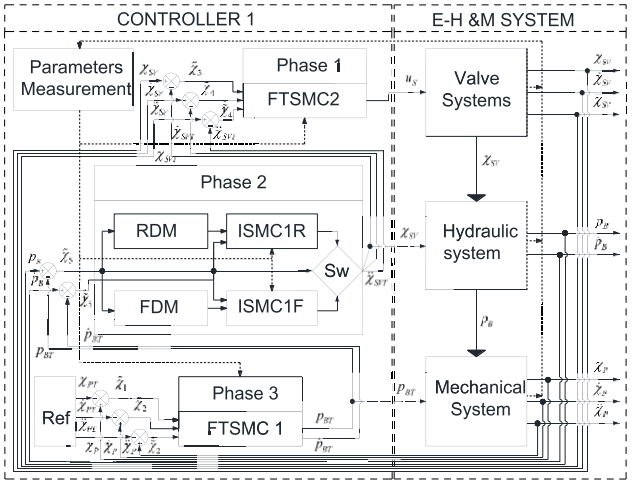

FIGURE 2. A multiphase control structure for abrupt acceleration tracking.

B. A NOVEL SWITCHING-TECHNIQUE-BASED CONTROL STRUCTURE FOR INSTANTANEOUS ACCELERATION TRACKING

Fig. 2 presents a three-phase finite-time convergence control structure. From the dynamic system (1) and (5–9), the system that controls acceleration (System 1) is considered a single-input and single-output (SISO) system with voltage u_S and actuator movement χ_P as its overall command input and output, respectively. The SISO system has three main subsystems, namely, a proportional directional servo valve, a hydraulic brake subsystem, and a pneumatic piston with a brake subsystem. Calculating the direct relationship between u_S and χ_P introduces a significant challenge in the application of a single nonlinear control algorithm because each subsystem is a nonlinear SISO system. This study then establishes a novel multiphase finite-time convergence structure of SMCs to control the entire system (Fig. 2). In Phase 1, the control input given to the servo valve accurately controls the spool movement. The precise displacement determines the pressure in the brake chamber and the friction force between the brake pad and piston rod in Phase 2. The exact brake pressure determines the actuator movement and guarantees the acceleration-tracking condition in Phase 3.

The imbalance in the installation of the proportional servo valve leads to different dynamic behaviors when two sides are working. These differences in turn lead to variations in fluid flow and in the hydraulic oil pressure. The mathematical model of the servo valve is therefore split into return and forward model dynamics, and the switched ISMC controllers of brake pressure are established. In the control process, the tracking error of the hydraulic brake pressure is transferred to the switching block (Sw), which determines the proper working dynamic model and control law.

The controllers are calculated as follows.

The system states are defined as

$\chi_1 = \chi_P, \chi_2 = \dot{\chi}_P, \chi_3 = \chi_{SV}, \chi_4 = \dot{\chi}_{SV}, \chi_5 = p_B, \chi_6 = p_S, \chi_7 = \chi_{PC}, \chi_8 = \dot{\chi}_{PC}$.

The reference values of the state variables are

$\chi_{1T} = \chi_{PT}, \chi_{2T} = \dot{\chi}_{PT}, \dot{\chi}_{2T} = \ddot{\chi}_{PT}, \chi_{3T} = \chi_{SVT}, \chi_{4T} = \dot{\chi}_{SVT}, \dot{\chi}_{4T} = \ddot{\chi}_{SVT}, \chi_{5T} = p_{BT}, \dot{\chi}_{5T} = \dot{p}_{BT}, \chi_{6T} = p_{ST}, \dot{\chi}_{6T} = \dot{p}_{ST}, \chi_{7T} = \chi_{PCT}, \chi_{8T} = \dot{\chi}_{PCT}, \dot{\chi}_{8T} = \ddot{\chi}_{PCT}$.

The tracking errors between the system states and their desired values are

$$\begin{aligned} \tilde{\chi}_i &= \chi_i - \chi_{iT}, \quad for\ i = 1 \ldots 8, \\ \dot{\tilde{\chi}}_i &= \dot{\chi}_i - \dot{\chi}_{iT}, \quad for\ i = 2, 4, 5, 6, 8. \end{aligned}$$

Following Lemma 1, the controller for high-accuracy acceleration tracking is computed as

$$\begin{aligned} &p_{BT}(t) \\ &= -(m_P + m_L)\left(\mu_{d0}(n_v e^{-m_v \dot{\chi}_P} + 1)a_B\right)^{-1} \\ &\quad \times \begin{pmatrix} -\mu_{2P}\,\mathrm{sgn}\left(\zeta_{fP}\right)^{\varepsilon_P} + \ddot{\chi}_{PT} - \mu_{3P}\,\mathrm{sgn}\left(\zeta_{fP}\right) \\ -\beta_{1P}\left(\dot{\chi}_1 - \dot{\chi}_{PT}\right) - (m_P + m_L)^{-1} a_P p_{P2} \\ -\mu_{1P}\zeta_{fP} - \beta_{2P}\dfrac{\alpha_P}{\gamma_P}\left(\dot{\chi}_1 - \dot{\chi}_{PT}\right)|\chi_1 - \chi_{PT}|^{\frac{\alpha_P}{\gamma_P}-1} \end{pmatrix} \\ &\quad - \left(\mu_{d0}(n_v e^{-m_v \dot{\chi}_P} + 1)a_B\right)^{-1} \\ &\quad \times \begin{pmatrix} \left(F_{fc0} + F_{fs0} e^{-|\chi_2|c_S^{-1}}\right) \\ +b_P\chi_2 + K_L\chi_1 + (a_P - a_R)p_{p1} \end{pmatrix}, \end{aligned} \tag{40}$$

$$\begin{aligned} &\zeta_{fP} \\ &= \beta_{1P}\tilde{\chi}_P + \beta_{2P}\,\mathrm{sgn}\left(\tilde{\chi}_P\right)^{\frac{\alpha}{\gamma}} + \dot{\tilde{\chi}}_P \\ &= \beta_{1P}\tilde{\chi}_1 + \beta_{2P}\,\mathrm{sgn}\left(\tilde{\chi}_1\right)^{\frac{\alpha_P}{\gamma_P}} + \tilde{\chi}_2 \\ &= \beta_{1P}\left(\chi_1 - \chi_{PT}\right) + \beta_{2P}\,\mathrm{sgn}\left(\chi_1 - \chi_{PT}\right)^{\frac{\alpha_P}{\gamma_P}} + \chi_2 - \dot{\chi}_{PT}. \end{aligned} \tag{41}$$

The controller for the spool position is

$$\begin{aligned} &\zeta_{fSV} \\ &= \beta_{1SV}\tilde{\chi}_{SV} + \beta_{2SV}\,\mathrm{sgn}\left(\tilde{\chi}_{SV}\right)^{\frac{\alpha_{SV}}{\gamma_{SV}}} + \dot{\tilde{\chi}}_{SV} \\ &= \beta_{1SV}\tilde{\chi}_3 + \beta_{2SV}\,\mathrm{sgn}\left(\tilde{\chi}_3\right)^{\frac{\alpha_{SV}}{\gamma_{SV}}} + \tilde{\chi}_4 \\ &= \beta_{1SV}\left(\chi_3 - \chi_{SVT}\right) + \beta_{2SV}\,\mathrm{sgn}\left(\chi_3 - \chi_{SVT}\right)^{\frac{\alpha_{SV}}{\gamma_{SV}}} \\ &\quad + \chi_4 - \dot{\chi}_{SVT}, \end{aligned} \tag{42}$$

$$\begin{aligned} &u_S(t) \\ &= \omega_{SV}^{-2} K_U^{-1} \begin{pmatrix} +\ddot{\chi}_{SVT} - \beta_{1SV}\left(\dot{\chi}_3 - \dot{\chi}_{SVT}\right) + 2\xi_{SV}\omega_{SV}^1\chi_4 \\ -\beta_{2SV}\dfrac{\alpha_{SV}}{\gamma_{SV}}\left(\dot{\chi}_3 - \dot{\chi}_{SVT}\right)|\chi_3 - \chi_{SVT}|^{\frac{\alpha_{SV}}{\gamma_{SV}}-1} \\ -\mu_{f1SV}\zeta_{fSV} - \mu_{f2SV}\,\mathrm{sgn}\left(\zeta_{fSV}\right)^{\varepsilon_{SV}} \\ +\chi_3\omega_{SV}^2 - \mu_{f3SV}\,\mathrm{sgn}\left(\zeta_{fSV}\right) \\ +4\Delta p\lambda_1 C_{d3}^2 D_S \chi_3 \omega_{SV}^2 \sin^{-1}\left(\dfrac{H_S}{D_S}\right)\cos(\theta_v) \end{pmatrix}. \end{aligned} \tag{43}$$

Based on Lemma 4, the control law for brake pressure in both cases is formulated as follows.

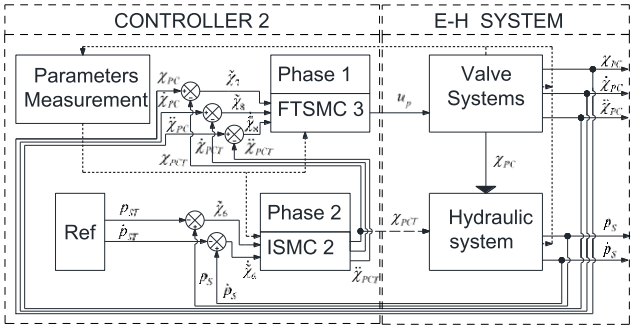

FIGURE 3. Control structure for the supply pressure.

In Case A, the level of surge in brake pressure is controlled by

$$\begin{aligned}\zeta_{iBA} &= \beta_{iBA}\int_0^t \tilde{\chi}_5 d\tau + \tilde{\chi}_5 \\ &= \beta_{iBA}\int_0^t (\chi_5 - p_{BT})\, d\tau + \chi_5 - p_{BT} \qquad (44)\end{aligned}$$

$$\begin{aligned}\chi_3 = &\begin{pmatrix} -\mu_{i1BA} V_B \left|\zeta_{iBA}(t)\right|^{\frac{1}{2}} \operatorname{sgn}(\zeta_{iBA}(t)) \\ -V_B \mu_{i2BA} \operatorname{sgn}(\zeta_{iBA}(t)) \\ +\dot{p}_{BT} V_B - \beta_{iBA} V_B (\chi_5 - p_{BT}) \end{pmatrix}^{-1} \\ &\times C_{d3}\pi D_{SV} \\ &\times \beta_E \sqrt{\frac{2}{\rho_H}\left|\left(1 - \frac{1.79\mu^{0.25}\rho_H^{0.75}Q_F^{1.75}l_{p1}}{\pi^{1.75}p_S d_p^{4.57}}\right)\chi_6 - \chi_5\right|}. \qquad (45)\end{aligned}$$

In Case B, the control law for reducing brake pressure is

$$\begin{aligned}\zeta_{iBB} &= \beta_{iBB}\int_0^t \tilde{\chi}_5 d\tau + \tilde{\chi}_5 \\ &= \beta_{iBB}\int_0^t (\chi_5 - p_{BT})\, d\tau + \chi_5 - p_{BT} \qquad (46)\end{aligned}$$

$$\begin{aligned}\chi_3 = &\begin{pmatrix} -\mu_{i1BB} V_B \left|\zeta_{iBB}(t)\right|^{\frac{1}{2}} \operatorname{sgn}(\zeta_{iBB}(t)) \\ -V_B \mu_{i2BB} \operatorname{sgn}(\zeta_{iBB}(t)) \\ +\dot{p}_{BT} V_B - \beta_{iBB} V_B (\chi_5 - p_{BT}) \end{pmatrix}^{-1} \\ &\times \left(-C_{d4}\pi D_{SV}\beta_E \sqrt{2(\chi_5 - p_T)\frac{1}{\rho_H}}\right). \qquad (47)\end{aligned}$$

C. MECHANISM FOR CONTROLLING SUPPLY HYDRAULIC PRESSURE

Fig. 3 presents the two-phase structure for controlling the inlet hydraulic pressure (System 1).

The command signal for the proportional pressure control valve is calculated as

$$\begin{aligned}&\zeta_{fPC} \\ &= \beta_{1PC}\tilde{\chi}_{PC} + \beta_{2PC}\operatorname{sgn}(\tilde{\chi}_{PC})^{\frac{\alpha_{PC}}{\gamma_{PC}}} + \dot{\tilde{\chi}}_{PC} \\ &= \beta_{1PC}\tilde{\chi}_7 + \beta_{2PC}\operatorname{sgn}(\tilde{\chi}_7)^{\frac{\alpha_{PC}}{\gamma_{PC}}} + \dot{\tilde{\chi}}_8 \\ &= \chi_8 - \dot{\chi}_{PCT} + \beta_{1PC}(\chi_7 - \chi_{PCT}) \\ &\quad + \beta_{2PC}\operatorname{sgn}(\chi_7 - \chi_{PCT})^{\frac{\alpha_{PC}}{\gamma_{PC}}}, \qquad (48)\end{aligned}$$

$$\begin{aligned}&u_{PC}(t) \\ &= -K_{PC}^{-1}\begin{pmatrix} +m_{PC}^{-1}b_{PC}\chi_8 - m_{PC}^{-1}\dfrac{\pi C_f D_{PC}^2}{4}(\chi_6 - p_{h3}) \\ -\mu_{f1PC}\zeta_{fPC} - \mu_{f2PC}\operatorname{sgn}\left(\zeta_{fPC}\right)^{\varepsilon_{PC}} \\ +c_{PC}\chi_7 - \mu_{f3PC}\operatorname{sgn}\left(\zeta_{fPC}\right) + \ddot{\chi}_{PCT} \\ -\beta_{1PC}(\dot{\chi}_7 - \dot{\chi}_{PCT}) - \beta_{2PC}\dfrac{\alpha_{PC}}{\gamma_{PC}} \\ (\dot{\chi}_7 - \dot{\chi}_{PCT})\left|\chi_7 - \chi_{PCT}\right|^{\frac{\alpha_{PC}}{\gamma_{PC}}-1}\end{pmatrix}. \qquad (49)\end{aligned}$$

When the pressure control valve is opened, $sg(-\chi_{PC}) = -\chi_{PC}$, and the desired displacement of its spool is determined by

$$\begin{aligned}&\zeta_{iS} \\ &= \beta_{iS}\int_0^t \tilde{\chi}_6 d\tau + \tilde{\chi}_6 \\ &= \beta_{iS}\int_0^t (\chi_6 - p_{ST})\, d\tau + \chi_6 - p_{ST} \qquad (50)\end{aligned}$$

$$\begin{aligned}&\chi_{PCT}(t) \\ &= V_S\left(\beta_E C_{d2}\pi D_{pc}\sqrt{(\chi_6 - p_{h3})\frac{1}{\rho_H}}\right)^{-1} \\ &\quad \times \begin{pmatrix} -\dfrac{\beta_E}{V_S}C_{d1}A_F\sqrt{2(p_{h1} - \chi_6)\dfrac{1}{\rho_H}} \\ +\dot{p}_{ST} - \mu_{i1S}\left|\zeta_{iS}(t)\right|^{\frac{1}{2}}\operatorname{sgn}(\zeta_{iS}(t)) \\ -\mu_{i2S}\operatorname{sgn}(\zeta_{iS}(t)) - \beta_{iS}(\chi_6 - p_{ST}) \\ +\dfrac{\beta_E}{V_S}C_{d3}\pi D_{SV}\, sn(\chi_3)\sqrt{\dfrac{2}{\rho_H}\left|\begin{matrix}(1-\eta_H)\chi_6 \\ -\chi_5\end{matrix}\right|}\end{pmatrix}. \qquad (51)\end{aligned}$$

The symbols and definitions involved in the proposed control scheme are presented in Table 1.

D. TIME-CONVERGENCE ANALYSES

Given the control laws (40)–(51) and the control structure in Figs. 2 and 3, Phase 2 converges only after the convergence of Phase 1 and so on. Therefore, the convergence time of each phase is always longer than that of the previous phase and shorter than that of the later phase. The convergence time of each phase is calculated by summing the convergence times of all previous and current phases.

TABLE 1. Symbols used throughout the paper.

Symbol	DESCRIPTION
a_p, a_b	Effective areas of the pneumatic piston and brake piston
a_R	Cross-section area of the piston rod
A_S	Directional valve size constant
b_P	Equivalent piston-cylinder friction coefficient
c_s	Friction force constant
C_{d3}, C_{d4}	Discharge coefficients of the directional valve for forward direction and for backward direction, respectively
D_S	Spool's diameter
F_{fc0}, F_{fs0}	Coulomb and static friction, respectively
H_S	Outlet port height
K_L	Equivalent load stiffness
K_U	Directional valve gain
l_{p1}	Length of high-pressure hydraulic pipe
n_v	Multiplication factor of friction
m_v	Parametric coefficient of friction
m_P, m_L	Mass of the piston and the external load, respectively
p_{ST}	Reference value of supply pressure
μ_{d0}	Piston-brake steady-state friction coefficient
μ_{d1}	Equivalent piston-brake friction coefficient
ρ_H	Equivalent hydraulic efficiency
ω_{sv}	Hydraulic directional valve damping ratio
β_E	Effective hydraulic bulk modulus
V_B	Brake chamber volume
μ	Hydraulic fluid dynamic viscosity
η_H	Equivalent hydraulic efficiency
ξ_{SV}, ω_{SV}	Natural frequency and damping ratio of the hydraulic directional valve
λ_f	Adjustment coefficient
θ	Jet angle
x_i, x_f	The index "i" and "f" denote the variables or functions of the first and second order subsystem in the ISMC and FTSMC.
ζ	Presenting for sliding variables
μ, α, β, γ	Denoting the controller coefficients
χ, χ_T	χ denotes the system states and the index "T" represents the target trajectory of the state variable χ

Based on (51–53), the convergence time of the entire SISO system is calculated as

$$T_C = \sum_{j=1}^{n} t_{rj}, \tag{52}$$

where n is the number of subsystems, and t_{rj} is the convergence period of thej^{th} phase.

Lemma 7: The times of convergence of supply pressure and actuator acceleration to their reference values are denoted by T_{C1} andT_{C2} (as in (54) and (53)), respectively.

$$T_{C2} = \left(\begin{array}{l} \gamma_{PC}\left(\beta_{1PC}\left(\gamma_{PC}-\alpha_{PC}\right)\right)^{-1} \\ .\ln\left(\left(\beta_{1PC}\left|\tilde{\chi}_{PC}\left(0\right)\right|^{\frac{\gamma_{PC}-\alpha_{PC}}{\gamma_{PC}}}+\beta_{2PC}\right)\beta_{2PC}^{-1}\right) \\ +2\delta_{iS}^{-1}\Upsilon_{iS}^{\frac{1}{2}}(0) \end{array} \right). \tag{53}$$

$$T_{C1} = \ln\left(\begin{array}{l} \left(\beta_1\left|\tilde{\chi}_P\left(0\right)\right|^{\frac{\gamma_P-\alpha_P}{\gamma_P}}+\beta_{2P}\right)^{\frac{\gamma_P}{\beta_{1P}\left(\gamma_P-\alpha_P\right)}} \\ \left(\beta_{1SV}\left|\tilde{\chi}_{SV}\left(0\right)\right|^{\frac{\gamma_{SV}-\alpha_{SV}}{\gamma_{SV}}}+\beta_{2SV}\right)^{\frac{\gamma_{SV}}{\beta_{1SV}\left(\gamma_{SV}-\alpha_{SV}\right)}} \\ \beta_{2P}^{\frac{\gamma_P}{\beta_{1P}\left(\alpha_P-\gamma_P\right)}}\beta_{2SV}^{\frac{\gamma_{SV}}{\beta_{1SV}\left(\alpha_{SV}-\gamma_{SV}\right)}} \end{array} \right). \\ +2\delta_{iB}^{-1}\Upsilon_{iB}^{\frac{1}{2}}(0) \tag{54}$$

Proof: The proof of Lemma 7 is given in the Appendix.

Based on these calculations and analyses, the times for the inlet supply pressure (p_S) and hydraulic pressure in the brake chamber (p_B) to be tracked to their desired trajectories (p_{ST} and p_{BT}) are denoted by T_{C2} and $\gamma_P\left(\beta_{1P}\left(\gamma_P-\alpha_P\right)\right)^{-1}\ln\left(\left(\begin{array}{l}\beta_1\left|\tilde{\chi}_P\left(0\right)\right|^{\frac{\gamma_P-\alpha_P}{\gamma_P}} \\ +\beta_{2P}\end{array}\right)\beta_{2P}^{-1}\right)+$ $\left|\zeta_{iB}\left(0\right)\right|\mu_{iB}^{-1}$, respectively. These convergence periods follow the error tracking of spool movements of the pressure control and proportional directional valves ($\tilde{\chi}_3$, $\tilde{\chi}_4$, $\dot{\tilde{\chi}}_4$ and $\tilde{\chi}_7$, $\tilde{\chi}_8$, $\dot{\tilde{\chi}}_8$) converged to the original point at times $\gamma_{PC}\beta_{1PC}^{-1}\left(\gamma_{PC}-\alpha_{PC}\right)^{-1}$ $\ln\left(\left(\beta_{1PC}\left|\tilde{\chi}_{PC}\left(0\right)\right|^{\frac{\gamma_{PC}-\alpha_{PC}}{\gamma_{PC}}}+\beta_{2PC}\right)\beta_{2PC}^{-1}\right)$ and $\gamma_{SV}\beta_{1SV}^{-1}\left(\gamma_{SV}-\alpha_{SV}\right)^{-1}\ln\left(\beta_{1SV}\left|\tilde{\chi}_{SV}\left(0\right)\right|^{\frac{\gamma_{SV}-\alpha_{SV}}{\gamma_{SV}}}\right.$ $\left.+\beta_{2SV}\right)\beta_{2SV}^{-1}$, respectively. Eventually, the time for the pneumatic actuator acceleration ($\ddot{\chi}_P$) to consolidate its reference curb is denoted by T_{C1}.

IV. SIMULATION AND INDUSTRIAL IMPLEMENTATION

A. NUMERICAL SIMULATION

This section focuses on controlling the acceleration of the actuator (System 1).

The system parameters for acceleration tracking are

$m_P = 75$ kg, $m_L = 951$ kg, $b_P = 579$ Ns/m, $K_L = 755$ N/m, $F_{fc0} = 1595$ N, $F_{fs0} = 1375$ N, $a_P = 189 \times 10^{-4}$ m^2, $a_R = 87 \times 10^{-4}$ m^2, $a_B = 245 \times 10^{-4}$, $\mu_{d0} = 0.45$, $n_v = 0, 012$, $m_v = 0.00035$, $c_s = 3.5$, $\mu_{d1} = 0.471$, $\rho_H = 0.880$ g/cm^3, $p_{ST} = 100$ bar, $C_{d3} = 0.67$, $\omega_{sv} = 0.02$ m, $\beta_E = 1.39 \times 10^9$ N/ m^2,

$V_B = 37.397115 \times 10^{-6}$ m^3, $l_{p1} = 3.95$ m, $d_p = 0.006$ m, $\mu = 2.4 \times 10^{-2}$, $\eta_H = 0.913$, $C_{d4} = 0.616$, $\xi_{SV} = 0.7$, $\omega_{SV} = 1160$ rad/s, $D_S = 7.145 \times 10^{-3}$ m, $H_S = 4 \times 10^{-3}$ m,$\lambda_f = 0.0915 \times 10^{-6}$, $\lambda_1 = 0.9$, $\theta = 60°$, $K_U = 3.4 \times 10^{-5}$ V/m, and $A_S = 4.25 \times 10^{-3}$ m.

Figs. 4 to 14 show the numerical simulations conducted within a 0.1 s control period.

Figs. 4 to 6 illustrate the movement of the actuator controlled by three-phase conventional SMCs (green dotted line) and FTSMCs combined with ISMC (FSTSMCs) (violet dashed line). In the first half of the simulation, both controllers demonstrate an effective tracking performance with smooth and non-step sinusoidal patterns, but these controllers demonstrate different properties 0.05 s later. Based on the practical working conditions, a composite pulse disturbance

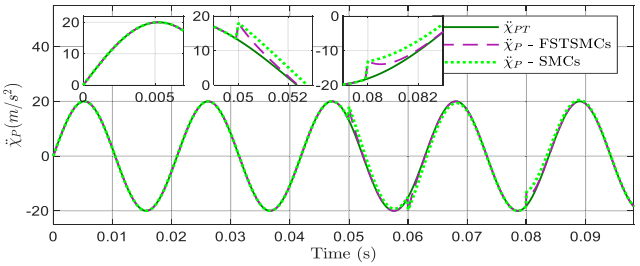

FIGURE 4. Acceleration tracking.

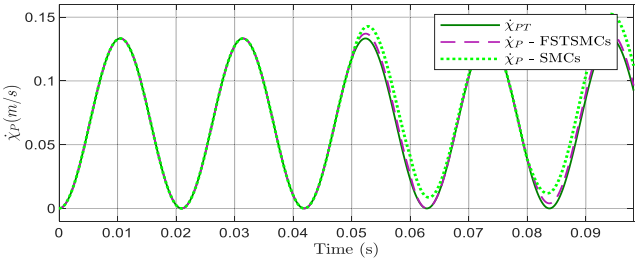

FIGURE 5. Velocity tracking.

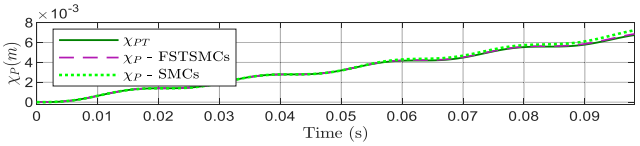

FIGURE 6. Displacement tracking.

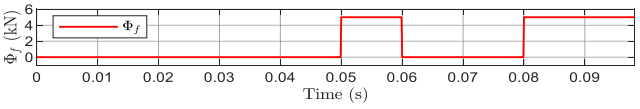

FIGURE 7. Composite disturbance.

(Fig. 7) is applied to the mechanical system (Phase 3) of the controller, after which piston accelerations are deflected off their reference curbs. Given that both controllers are robust, they force the actuator acceleration to return to a sinusoidal curve as shown in Fig. 4. For a conventional SMC, the acceleration does not return to its desired curve within 0.002 s. By contrast, the satisfactory disturbance rejection feature of FTSMC ensures that the acceleration can return to this curve within 0.0013 s. However, the position and velocity tracking errors accumulate to a larger value at the end of the simulation. The reference trajectory of brake pressure, which is roughly proportional to negative acceleration (green line in Fig. 4), is precisely tracked (violet line in Fig. 8). The shape of the desired spool position is roughly and continuously sinusoidal and is accurately tracked by the controlled spool displacement in Phase 1.

When tracking the pulse profile (Figs. 10 to 14), the controllers demonstrate different responses. Given the high level of acceleration (exceeding 11 m/s^2), the conventional SMC forces the actuator acceleration to its target within 0.04 s,

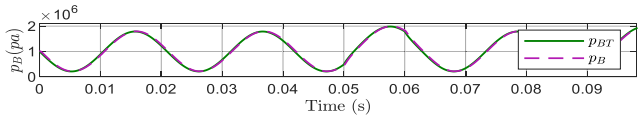

FIGURE 8. Brake pressure control.

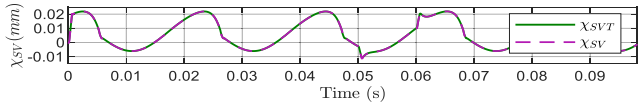

FIGURE 9. Spool displacement control.

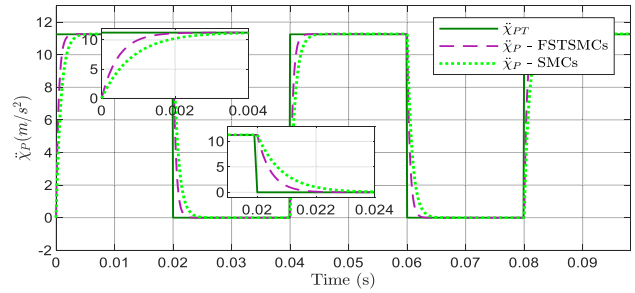

FIGURE 10. Acceleration tracking.

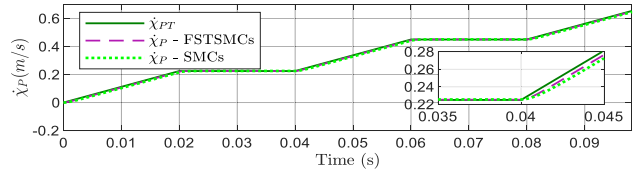

FIGURE 11. Velocity tracking.

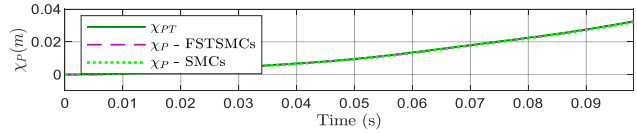

FIGURE 12. Displacement tracking.

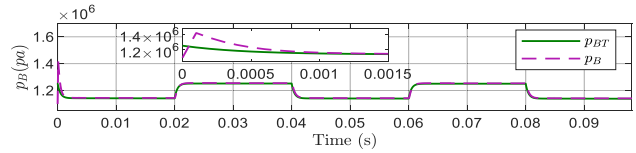

FIGURE 13. Brake pressure control.

which is approximately twice longer than the convergence time of FTSMC.

B. INDUSTRIAL IMPLEMENTATION

Fig. 15 presents the industrial platform, and Figs. 16 to 24 present the experimental results. With the command signal provided in Fig. 16, all movements (red lines) of the proportional servo valve spool are controlled as shown in Fig. 17. As a result, the hydraulic brake pressure (red lines) converges

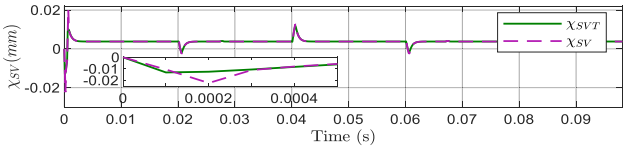

FIGURE 14. Spool postion control.

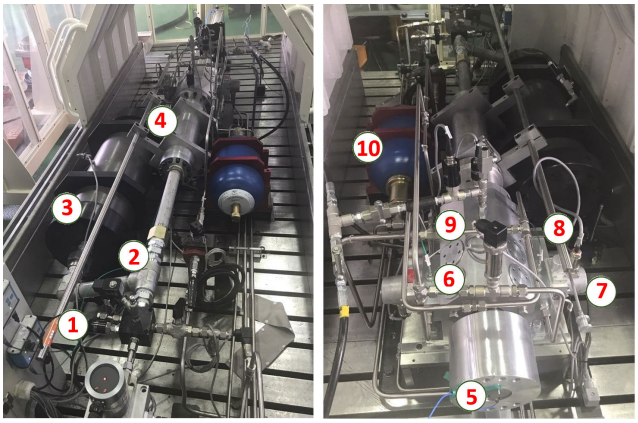

FIGURE 15. Experimental HEHPA system configuration: (1) Pneumatic pressure sensor, (2) pneumatic pipe, (3) air tank (150 bar), (4) pneumatic cylinder, (5) accelerometer, (6) hydraulic pressure sensor, (7) hydraulic proportional servo valve, (8) LVDT position sensor, (9) hydraulic brake system, and (10) hydraulic bladder accumulator.

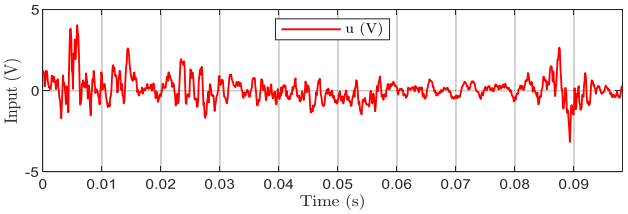

FIGURE 16. Command input.

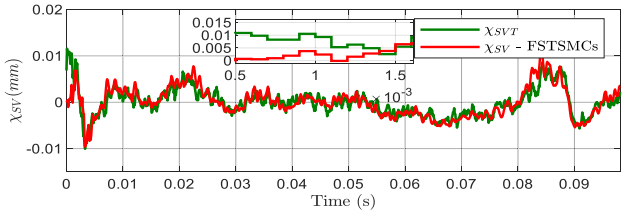

FIGURE 17. Control the spool displacement.

to its desired values (green lines; Fig. 18). Consequently, the piston movement, acceleration, velocity, and position (red lines) are tracked to their reference values.

The trajectory of actuator acceleration in the converged period has change rules that are roughly inversed with brake pressure variation in the experimental results. Moreover, the reduction in brake pressure coincides with the positive value of the servo valve spool displacement. Therefore, the dynamic system modeling that involves (1) and (5-9) is deemed reliable.

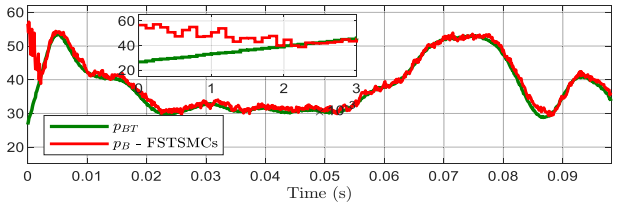

FIGURE 18. Control the brake pressure.

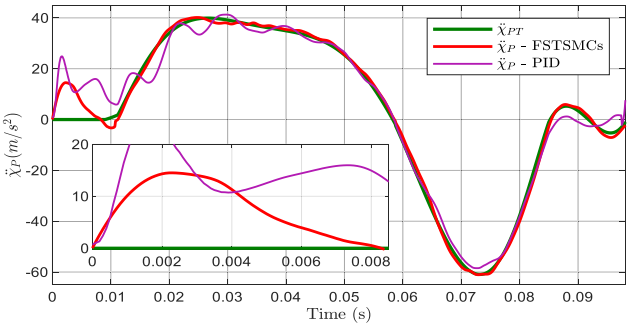

FIGURE 19. High-accuracy acceleration tracking.

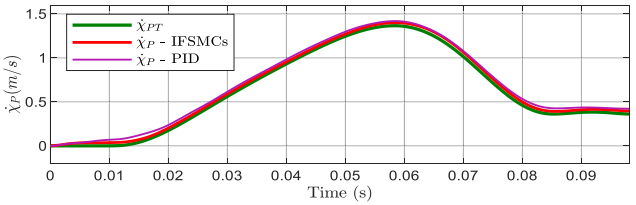

FIGURE 20. Piston velocity tracking.

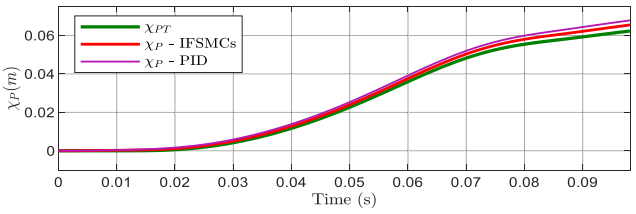

FIGURE 21. Piston postion tracking.

The convergence times of three phases, namely, spool position, brake pressure, and piston acceleration, are 0.0014, 0.0019, and 0.0068 s, respectively. These finite time periods are appropriate for the order of convergence times analyzed in Section 3.4 and the numerical simulation results in Figs. 10, 13, and 14.

Remark 1: This study presents a relatively new problem and approach in actuator control (rapid acceleration tracking control). The greatest challenges faced in this work lie in the design and setup of a complex hybrid system where devices are required to work at extremely high speeds and resolutions. Furthermore, the parameters of this system greatly vary and are extremely sensitive when the piston rod moves at a shock acceleration. The control accuracy reported in this work is considerably higher than those reported in previous studies

that only focus on single fluid-power (hydraulic or pneumatic) actuators, such as [62], by comparing tracking errors reported within short periods.

Remark 2: Using the same approach, the control structure is designed to be applicable to a variety of systems that have multiple series subsystems, such as hydraulic actuator systems (including valves, hydraulic subsystems, and actuators) and industrial excavators (including valves, hydraulic parts, actuator subsystems, and links).

V. CONCLUSION

An innovative hybrid platform with a technically appropriate combination of electrohydraulic, pneumatic, and mechanical subsystems is presented in this paper. This study focuses on the sudden acceleration-tracking control of an actuator. An advanced control structure with a switching mechanism is developed based on a nonlinear dynamic model. The robust and powerful convergence properties of the proper control strategy are investigated via numerical simulations. The controller not only overcomes the effects of internal uncertainties and external disturbance but also drives the actuator to follow the expected acceleration–time profile. This controller also forces the system state variables, including spool position and brake pressure, to their desired trajectories, thereby improving the quality and safety of the control process. The effectiveness of this approach is experimentally validated via an industrial implementation. Given that the proposed system is greatly affected by uncertainties, our future work shall focus on the robustness of this controller by combining the control law with adaptive algorithms.

ACKNOWLEDGMENT

(Quoc-Dong Hoang and Vinicio Alejandro Rosas-Cervantes are co-first authors.)

APPENDIX

PROOF OF LEMMA 7

From the control law and sliding surface in Lemma 1, the convergence time of each phase FTSMC [59]–[61] is determined by

$$\begin{aligned} t_{fr} &= -\int_{\tilde{\chi}_1(t=0)}^{\tilde{\chi}_1(t=t_{fr})} \left(\beta_1 \tilde{\chi}_1(t) + \beta_2 \left(\tilde{\chi}_1(t)\right)^{\frac{\alpha}{\gamma}}\right)^{-1} d\tilde{\chi}_1(t) \\ &= -\int_{\tilde{\chi}_1(t=0)}^{\tilde{\chi}_1(t=t_{fr})} \xi\left(\tilde{\chi}_1(t)\right) d\tilde{\chi}_1(t). \end{aligned} \tag{55}$$

Based on (14), function $F_d\left(\tilde{\chi}_1(t)\right)$ is given by

$$\xi\left(\tilde{\chi}_1(t)\right) = \begin{cases} \beta_1 \tilde{\chi}_1(t) + \beta_2 \left(\tilde{\chi}_1(t)\right)^{\frac{\alpha}{\gamma}}, & \tilde{\chi}_1(t) > 0 \\ 0, & \tilde{\chi}_1(t) = 0 \\ -\beta_1 \tilde{\chi}_1(t) - \beta_2 \left(-\tilde{\chi}_1(t)\right)^{\frac{\alpha}{\gamma}}, & \tilde{\chi}_1(t) < 0. \end{cases} \tag{56}$$

In the case of $\tilde{\chi}_1(t) \geq 0$, the convergence period can be computed as

$$t_{fr} = \gamma\left(\beta_1(\gamma-\alpha)\right)^{-1} \ln\left(\left(\beta_1\left(\tilde{\chi}_1(0)\right)^{\frac{\gamma-\alpha}{\gamma}} + \beta_2\right)\beta_2^{-1}\right) \tag{57}$$

based on

$$\begin{aligned} t_{fr} = &-\int_{\tilde{\chi}_1(t=0)}^{\tilde{\chi}_1(t=t_{fr})} \alpha\left(\gamma\tilde{\chi}_1(t)\,\beta_1\left(\frac{\alpha-\gamma}{\gamma}\right)\right)^{-1} d\tilde{\chi}_1(t) \\ &+ \int_{\tilde{\chi}_1(t=0)}^{\tilde{\chi}_1(t=t_{fr})} \left(\left(\left(\frac{\alpha-\gamma}{\gamma}\right)\left(\beta_1\tilde{\chi}_1(t) + \beta_2\left(\tilde{\chi}_1(t)\right)^{\frac{\alpha}{\gamma}}\right)\right)^{-1} \right. \\ &\left. \beta_1\left(\beta_1 + \beta_2\frac{\alpha}{\gamma}\left(\tilde{\chi}_1(t)\right)^{\frac{\alpha-\gamma}{\gamma}}\right)\right) \\ &\times d\tilde{\chi}_1(t), \end{aligned} \tag{58}$$

and

$$\begin{aligned} t_{fr} = &\int_{\beta_1\tilde{\chi}_1(0)+\beta_2\left(\tilde{\chi}_1(0)\right)^{\frac{\alpha}{\gamma}}}^{\beta_1\tilde{\chi}_1(t_{fr})+\beta_2\left(\tilde{\chi}_1(t_{fr})\right)^{\frac{\alpha}{\gamma}}} \left(\beta_1\left(\frac{\alpha-\gamma}{\gamma}\right)\xi(t)\right)^{-1} d\xi(t) \\ &- \int_{\tilde{\chi}_1(0)}^{\tilde{\chi}_1(t_{fr})} \left(\gamma\tilde{\chi}_1(t)\,\beta_1\left(\frac{\alpha-\gamma}{\gamma}\right)\right)^{-1} d\tilde{\chi}_1(t), \end{aligned} \tag{59}$$

where $\alpha < \gamma < 2\alpha$.

These equations are derived from (60), as shown at the top of the next page.

In the case of $\tilde{\chi}_1(t) < 0$, the convergence period can be computed as

$$t_{fr} = \gamma\left(\beta_1(\gamma-\alpha)\right)^{-1} \ln\left(\left(\beta_1\left(-\tilde{\chi}_1(0)\right)^{\frac{\gamma-\alpha}{\gamma}} + \beta_2\right)\beta_2^{-1}\right) \tag{61}$$

because $\xi\left(\tilde{\chi}_1(t)\right)$ is an odd function, and

$$t_{fr} = -\int_{-\tilde{\chi}_1(t=0)}^{-\tilde{\chi}_1(t=t_{fr})} \left(-\beta_1\tilde{\chi}_1(t) - \beta_2\left(\tilde{\chi}_1(t)\right)^{\frac{\alpha}{\gamma}}\right)^{-1} d\left(-\tilde{\chi}_1(t)\right). \tag{62}$$

For arbitrary values of $\tilde{\chi}_1(t) \in \Re$, the convergence time is computed as

$$t_{fr} = \gamma\left(\beta_1(\gamma-\alpha)\right)^{-1} \ln\left(\left(\beta_1\left|-\tilde{\chi}_1(0)\right|^{\frac{\gamma-\alpha}{\gamma}} + \beta_2\right)\beta_2^{-1}\right). \tag{63}$$

Following Lemma 6, the convergence time is

$$t_{ic} \leq 2\delta_i^{-1}\Upsilon_i^{\frac{1}{2}}(0), \tag{64}$$

and the convergence time for controlling the supply pressure is

$$\begin{aligned} T_{C2} &= t_{frPC} + t_{icS} \\ &= \left(\gamma_{PC}\left(\beta_{1PC}\left(\gamma_{PC} - \alpha_{PC}\right)\right)^{-1} \cdot \right. \\ &\quad \left. \ln\left(\left(\beta_{1PC}\left|\tilde{\chi}_{PC}(0)\right|^{\frac{\gamma_{PC}-\alpha_{PC}}{\gamma_{PC}}} + \beta_{2PC}\right)\beta_{2PC}^{-1}\right)\right) \end{aligned}$$

$$t_{fr} = \int_{\tilde{\chi}_1(t=0)}^{\tilde{\chi}_1(t=t_{fr})} \left(\begin{array}{l} \left(\left(\beta_1 \tilde{\chi}_1(t) + \beta_2 \left(\tilde{\chi}_1(t) \right)^{\frac{\alpha}{\gamma}} \right) \beta_1 (\alpha - \gamma) \tilde{\chi}_1(t) \gamma \right)^{-1} \\ . \left(\begin{array}{l} \gamma \tilde{\chi}_1(t) \left(\beta_1 + \beta_2 \frac{\alpha}{\gamma} \left(\tilde{\chi}_1(t) \right)^{\frac{\alpha-\gamma}{\gamma}} \right) \\ -\alpha \left(\beta_1 \tilde{\chi}_1(t) + \beta_2 \left(\tilde{\chi}_1(t) \right)^{\frac{\alpha}{\gamma}} \right) \end{array} \right) \end{array} \right) d\tilde{\chi}_1(t)$$

$$= \int_{\tilde{\chi}_1(t=0)}^{\tilde{\chi}_1(t=t_{fr})} \left(\begin{array}{l} \left(\beta_1 \left(\frac{\alpha-\gamma}{\gamma} \right) \right)^{-1} \left(\beta_1 + \beta_2 \frac{\alpha}{\gamma} \left(\tilde{\chi}_1(t) \right)^{\frac{\alpha-\gamma}{\gamma}} \right) \\ \left(\beta_1 \tilde{\chi}_1(t) + \beta_2 \left(\tilde{\chi}_1(t) \right)^{\frac{\alpha}{\gamma}} \right)^{-1} \\ -\left(\gamma \tilde{\chi}_1(t) \right)^{-1} \alpha \left(\beta_1 \left(\frac{\alpha-\gamma}{\gamma} \right) \right)^{-1} \end{array} \right) d\tilde{\chi}_1(t). \quad (60)$$

$$+ 2\delta_{iS}^{-1} \Upsilon_{iS}^{\frac{1}{2}}(0). \quad (65)$$

For SISO system 1, the convergence period is calculated as

$$T_{C1} = t_{frP} + t_{frSV} + t_{icB}. \quad (66)$$

$$T_{C1} = \left(\begin{array}{l} \left(\begin{array}{l} \gamma_P \left(\beta_{1P} \left(\gamma_P - \alpha_P \right) \right)^{-1} \\ . \ln \left(\left(\beta_1 \left| \tilde{\chi}_P(0) \right|^{\frac{\gamma_P - \alpha_P}{\gamma_P}} + \beta_{2P} \right) \beta_{2P}^{-1} \right) \end{array} \right) \\ + 2\delta_{iB}^{-1} \Upsilon_{iB}^{\frac{1}{2}}(0) \\ \left(\begin{array}{l} \gamma_{SV} \left(\beta_{1SV} \left(\gamma_{SV} - \alpha_{SV} \right) \right)^{-1} \\ . \ln \left(\beta_{1SV} \left| \tilde{\chi}_{SV}(0) \right|^{\frac{\gamma_{SV} - \alpha_{SV}}{\gamma_{SV}}} + \beta_{2SV} \right) \beta_{2SV}^{-1} \end{array} \right) \end{array} \right). \quad (67)$$

This computation ascertains the accuracy of T_{C1} in (54). The proof of Lemma 7 is therefore completed.

REFERENCES

[1] L. Xiaochuan, S. Xiasheng, G. Jun, and M. Rangke, "Crash simulation and drop test of civil airplane fuselage section," in *Proc. Int. Conf. Mech. Sci., Electric Eng. Comput. (MEC)*, Dec. 2013, pp. 3017–3021.

[2] X. Ma, P. K. Wong, J. Zhao, and Z. Xie, "Cornering stability control for vehicles with active front steering system using T-S fuzzy based sliding mode control strategy," *Mech. Syst. Signal Process.*, vol. 125, pp. 347–364, Jun. 2019.

[3] Y. Sun, X. Sun, J. Rong, and Y. Tai, "Development of energy absorbing refuge island using crash simulation," in *Proc. Int. Conf. Transp., Mech., Electr. Eng. (TMEE)*, Dec. 2011, pp. 1012–1015.

[4] T.-L. Teng, P.-H. Chang, C.-C. Liang, and D.-A. Fung, "Application of crash pulse on the car crashworthiness design," *Adv. Mech. Eng.*, vol. 9, no. 9, pp. 1–8, Sep. 2017.

[5] M. Du, D. Zhao, T. Ni, L. Ma, and S. Du, "Output feedback control for active suspension electro-hydraulic actuator systems with a novel sampled-data nonlinear extended state observer," *IEEE Access*, vol. 8, pp. 128741–128756, Jul. 2020.

[6] B. Rouzbeh, G. M. Bone, G. Ashby, and E. Li, "Design, implementation and control of an improved hybrid pneumatic-electric actuator for robot arms," *IEEE Access*, vol. 7, pp. 14699–14713, Jan. 2019.

[7] L. A. Tuan, J.-J. Kim, S.-G. Lee, T.-G. Lim, and L. C. Nho, "Second-order sliding mode control of a 3D overhead crane with uncertain system parameters," *Int. J. Precis. Eng. Manuf.*, vol. 15, no. 5, pp. 811–819, May 2014.

[8] L. A. Tuan, S.-G. Lee, L. C. Nho, and D. H. Kim, "Model reference adaptive sliding mode control for three dimensional overhead cranes," *Int. J. Precis. Eng. Manuf.*, vol. 14, no. 8, pp. 1329–1338, Aug. 2013.

[9] L. A. Tuan, H. M. Cuong, P. V. Trieu, L. C. Nho, V. D. Thuan, and L. V. Anh, "Adaptive neural network sliding mode control of shipboard container cranes considering actuator backlash," *Mech. Syst. Signal Process.*, vol. 112, pp. 233–250, Nov. 2018.

[10] D. B. Pham and S.-G. Lee, "Aggregated hierarchical sliding mode control for a spatial ridable ballbot," *Int. J. Precis. Eng. Manuf.*, vol. 19, no. 9, pp. 1291–1302, Sep. 2018.

[11] M. A. Qureshi, I. Ahmad, and M. F. Munir, "Double integral sliding mode control of continuous gain four quadrant quasi-Z-source converter," *IEEE Access*, vol. 6, pp. 77785–77795, Dec. 2018.

[12] J. Li, H. Guo, H. Zhang, and Z. Yan, "Double-loop structure integral sliding mode control for UUV trajectory tracking," *IEEE Access*, vol. 7, pp. 101620–101632, Jun. 2019.

[13] A. T. Vo and H.-J. Kang, "Neural integral non-singular fast terminal synchronous sliding mode control for uncertain 3-DOF parallel robotic manipulators," *IEEE Access*, vol. 8, pp. 65383–65394, Apr. 2020.

[14] Q. Hoang, S. Lee, and B. Dugarjav, "Super-twisting observer-based integral sliding mode control for tracking the rapid acceleration of a piston in a hybrid electro-hydraulic and pneumatic system," *Asian J. Control*, vol. 21, no. 1, pp. 483–498, Jan. 2019.

[15] A. S. S. Ianagui, P. C. De Mello, and E. A. Tannuri, "Robust output-feedback control in a dynamic positioning system via high order sliding modes: Theoretical framework and experimental evaluation," *IEEE Access*, vol. 8, pp. 91701–91724, May 2020.

[16] G. V. Lakhekar, L. M. Waghmare, P. G. Jadhav, and R. G. Roy, "Robust diving motion control of an autonomous underwater vehicle using adaptive neuro-fuzzy sliding mode technique," *IEEE Access*, vol. 8, pp. 109891–109904, Jun. 2020.

[17] Z. Shi, C. Deng, S. Zhang, Y. Xie, H. Cui, and Y. Hao, "Hyperbolic tangent function-based finite-time sliding mode control for spacecraft rendezvous maneuver without chattering," *IEEE Access*, vol. 8, pp. 60838–60849, Apr. 2020.

[18] T. Ma, L. Li, and H. Li, "Observer-based finite-time adaptive sliding mode control for Itô stochastic jump systems with actuator degradation," *IEEE Access*, vol. 8, pp. 18590–18600, Jan. 2020.

[19] M. Fu, T. Zhang, and F. Ding, "Adaptive finite-time PI sliding mode trajectory tracking control for underactuated hovercraft with drift angle constraint," *IEEE Access*, vol. 7, pp. 184885–184895, 2019.

[20] L. A. Tuan and S.-G. Lee, "Modeling and advanced sliding mode controls of crawler cranes considering wire rope elasticity and complicated operations," *Mech. Syst. Signal Process.*, vol. 103, pp. 250–263, Mar. 2018.

[21] H. Pan, G. Zhang, H. Ouyang, and L. Mei, "Novel fixed-time non-singular fast terminal sliding mode control for second-order uncertain systems based on adaptive disturbance observer," *IEEE Access*, vol. 8, pp. 126615–126627, 2020.

[22] A. T. Vo and H.-J. Kang, "A novel fault-tolerant control method for robot manipulators based on non-singular fast terminal sliding mode control and disturbance observer," *IEEE Access*, vol. 8, pp. 109388–109400, Jun. 2020.

[23] V.-C. Nguyen, A.-T. Vo, and H.-J. Kang, "A non-singular fast terminal sliding mode control based on third-order sliding mode observer for a class of second-order uncertain nonlinear systems and its application to robot manipulators," *IEEE Access*, vol. 8, pp. 78109–78120, Apr. 2020.

[24] Y. Tian, Y. Cai, and Y. Deng, "A fast nonsingular terminal sliding mode control method for nonlinear systems with fixed-time stability guarantees," *IEEE Access*, vol. 8, pp. 60444–60454, Mar. 2020.

[25] H. Pan, G. Zhang, H. Ouyang, and L. Mei, "A novel global fast terminal sliding mode control scheme for second-order systems," *IEEE Access*, vol. 8, pp. 22758–22769, Jan. 2020.

[26] H. Pan and W. Sun, "Nonlinear output feedback finite-time control for vehicle active suspension systems," *IEEE Trans. Ind. Informat.*, vol. 15, no. 4, pp. 2073–2082, Apr. 2019.

[27] H. Pan, W. Sun, H. Gao, and J. Yu, "Finite-time stabilization for vehicle active suspension systems with hard constraints," *IEEE Trans. Intell. Transp. Syst.*, vol. 16, no. 5, pp. 2663–2672, Oct. 2015.
[28] H. Behrouz, I. Mohammadzaman, and A. Mohammadi, "Robust static output feedback design with pole placement constraints for linear systems with polytopic uncertainties," *Trans. Inst. Meas. Control*, to be published, doi: 10.1177/0142331218823857.
[29] S. Roy, S. Baldi, and L. M. Fridman, "On adaptive sliding mode control without *a priori* bounded uncertainty," *Automatica*, vol. 111, Jan. 2020, Art. no. 108650.
[30] Y. Chang, Y. Wang, F. E. Alsaadi, and G. Zong, "Adaptive fuzzy output-feedback tracking control for switched stochastic pure-feedback nonlinear systems," *Int. J. Adapt. Control*, vol. 33, no. 10, pp. 1567–1582, 2019.
[31] L. Ma, X. Huo, X. Zhao, and G. D. Zong, "Observer-based adaptive neural tracking control for output-constrained switched MIMO nonstrict-feedback nonlinear systems with unknown dead zone," *Nonlinear Dyn.*, vol. 99, no. 2, pp. 1019–1036, Jan. 2020.
[32] M. P. Aghababa, "Finite time control of a class of nonlinear switched systems in spite of unknown parameters and input saturation," *Nonlinear Anal., Hybrid Syst.*, vol. 31, pp. 220–232, Feb. 2019.
[33] S. Roy and S. Baldi, "On reduced-complexity robust adaptive control of switched Euler–Lagrange systems," *Nonlinear Anal., Hybrid Syst.*, vol. 34, pp. 226–237, Nov. 2019.
[34] R. B. Walters, *Hydraulic and Electro-Hydraulic Control Systems*. Norwell, MA, USA: Kluwer, 2000.
[35] M. A. Aizerman, *Pneumatic and Hydraulic Control Systems: Seminar on Pneumohydraulic Automation*, 1st ed. Amsterdam, The Netherlands: Elsevier, 2017.
[36] H. Merrit, *Hydraulic Control Systems*. Hoboken, NJ, USA: Wiley, 1991.
[37] V. I. Utkin, *Sliding Modes in Control and Optimization*. Berlin, Germany: Springer, 2013.
[38] S. Haggag, D. Alstrom, S. Cetinkunt, and A. Egelja, "Modeling, control, and validation of an electro-hydraulic steer-by-wire system for articulated vehicle applications," *IEEE/ASME Trans. Mechatronics*, vol. 10, no. 6, pp. 688–692, Dec. 2005.
[39] X. Zheng, Y. Li, Z. Liu, and C. Wang, "Steady-state control strategy of VSC-HVDC transmission system based on full-order terminal sliding mode control method," *J. Eng.*, vol. 2019, no. 16, pp. 987–990, Mar. 2019.
[40] J. J. E. Slotine, J. K. Hedrick, and E. A. Misawa, "On sliding observers for nonlinear systems," in *Proc. Amer. Control Conf.*, 1986, pp. 1794–1800.
[41] V. Utkin and J. Shi, "Integral sliding mode in systems operating under uncertainty conditions," in *Proc. 35th IEEE Conf. Decis. Control*, vol. 4, Dec. 1996, pp. 4591–4596.
[42] F. Plestan, Ed., *Recent Trends in Sliding Mode Control*. London, U.K.: Institution Engineering Technology, 2016.
[43] L. Fridman, J. Moreno, and R. Iriarte, *Sliding Modes After the First Decade of the 21st Century: State of the Art*. Berlin, Germany: Springer, 2011.
[44] A. Polyakov and L. Fridman, "Stability notions and Lyapunov functions for sliding mode control systems," *J. Franklin Inst.*, vol. 351, no. 4, pp. 1831–1865, Apr. 2014.
[45] E. Moulay and W. Perruquetti, "Finite time stability and stabilization of a class of continuous systems," *J. Math. Anal. Appl.*, vol. 323, no. 2, pp. 1430–1443, Nov. 2006.
[46] A. Levant, "Finite-time stability and high relative degrees in sliding-mode control BT," in *Sliding Modes After the First Decade of the 21st Century*, L. Fridman, J. Moreno, and R. Iriarte, Eds. Berlin, Germany: Springer, 2012, pp. 59–92.
[47] A. T. Azar and Q. Zhu, *Advances and Applications in Sliding Mode Control Systems*. New York, NY, USA: Springer, 2014.
[48] J. A. Moreno and M. Osorio, "Strict Lyapunov functions for the super-twisting algorithm," *IEEE Trans. Autom. Control*, vol. 57, no. 4, pp. 1035–1040, Apr. 2012.
[49] C. Mu and C. Sun, "A new finite time convergence condition for super-twisting observer based on Lyapunov analysis," *Asian J. Control*, vol. 17, no. 3, pp. 1050–1060, May 2015.
[50] J. Zheng, H. Wang, Z. Man, J. Jin, and M. Fu, "Robust motion control of a linear motor positioner using fast nonsingular terminal sliding mode," *IEEE/ASME Trans. Mechatronics*, vol. 20, no. 4, pp. 1743–1752, Aug. 2015.
[51] L. A. Tuan, "Neural observer and adaptive fractional-order backstepping fast-terminal sliding-mode control of RTG cranes," *IEEE Trans. Ind. Electron.*, vol. 68, no. 1, pp. 434–442, Jan. 2021.
[52] V. A. Tuan and H.-J. Kang, "A new finite time control solution for robotic manipulators based on nonsingular fast terminal sliding variables and the adaptive super-twisting scheme," *J. Comput. Nonlinear Dyn.*, vol. 14, no. 3, Jan. 2019.
[53] A. T. Vo and H.-J. Kang, "An adaptive terminal sliding mode control for robot manipulators with non-singular terminal sliding surface variables," *IEEE Access*, vol. 7, pp. 8701–8712, Dec. 2019.
[54] J. D. Sanchez-Torres, A. Navarrete-Guzman, G. Rubio-Astorga, and A. G. Loukianov, "High order integral nested sliding mode control," in *Proc. 13th Int. Workshop Variable Struct. Syst. (VSS)*, Jun. 2014, pp. 1–5.
[55] V. I. Utkin, "Sliding mode control in dynamic systems," in *Proc. 32nd IEEE Conf. Decis. Control*, vol. 3, Dec. 1993, pp. 2446–2451.
[56] J.-J. E. Slotine and W. Li, *Applied Nonlinear Control*, vol. 199, no. 1. Upper Saddle River, NJ, USA: Prentice-Hall, 1991.
[57] H. K. Khalil, *Nonlinear Systems*, vol. 3. Upper Saddle River, NJ, USA: Prentice-Hall, 2002.
[58] A. Shiralkar and S. Kurode, "Generalized super-twisting algorithm for control of electro-hydraulic servo system," *IFAC-PapersOnLine*, vol. 49, no. 1, pp. 742–747, 2016.
[59] X. Yu and M. Zhihong, "Fast terminal sliding-mode control design for nonlinear dynamical systems," *IEEE Trans. Circuits Syst. I, Fundam. Theory Appl.*, vol. 49, no. 2, pp. 261–264, Feb. 2002.
[60] S. Yu, X. Yu, Z. Man, and Y. Feng, "On singularity free recursive fast terminal sliding mode control," in *Proc. Int. Workshop Variable Struct. Syst.*, Jun. 2008, pp. 163–166.
[61] C. U. Solis, J. B. Clempner, and A. S. Poznyak, "Fast terminal sliding-mode control with an integral filter applied to a van der pol oscillator," *IEEE Trans. Ind. Electron.*, vol. 64, no. 7, pp. 5622–5628, Jul. 2017.
[62] G. Wrat, M. Bhola, P. Ranjan, S. K. Mishra, and J. Das, "Energy saving and fuzzy-PID position control of electro-hydraulic system by leakage compensation through proportional flow control valve," *ISA Trans.*, vol. 101, pp. 269–280, Jun. 2020.

QUOC-DONG HOANG received the B.E. and M.S. degrees in mechanical engineering from Vietnam Maritime University, Hai Phong, Vietnam, in 2010 and 2014, respectively, and the Ph.D. (dissertation) degree in mechanical engineering from Kyung Hee University, Yongin, South Korea, in 2020. Since 2010, he has held a research and teaching positions with the Institute of Mechanical Engineering, Vietnam Maritime University. His research interests include nonlinear control, artificial intelligent control, and mechatronics.

VINICIO ALEJANDRO ROSAS-CERVANTES received the bachelor's degree in electromechanical engineering from the Escuela Politécnica del Ejército, Ecuador, in 2011. He is currently pursuing the combined master's and Ph.D. degree from the Mechanical Engineering Program, Kyung Hee University, South Korea. His research interests include mobile robotics, simultaneous mapping and localization, and control theory.

SOON-GEUL LEE received the B.E. degree in mechanical engineering from Seoul National University, Seoul, South Korea, in 1983, the M.S. degree in production engineering from KAIST, Seoul, in 1985, and the Ph.D. degree in mechanical engineering from the University of Michigan, USA, in 1993. Since 1996, he has been with the Department of Mechanical Engineering, Kyung Hee University, Yongin, South Korea, where he is currently working as a Professor. His research interests include robotics and automation, mechatronics, intelligent control, and biomechanics.

IHN-SIK WEON received the B.S. degree in mechanical engineering from the Engineering College, Korea University, South Korea, in 2014, and the M.S. and Ph.D. degrees in mechanical engineering from the Engineering College, Kyung Hee University, South Korea. Since 2019, he has been with the Unmanned System, LIG Nex1, where he is currently working as an Assistant Researcher. His main research interests include the control algorithm of autonomous vehicles, unmanned surface vessels, and intelligent assistance robots.

JAE-HWAN CHOI received the M.S. degree in mechanical engineering from Kyung Hee University, Yongin, South Korea, in 2015, where he is currently pursuing the Ph.D. degree in mechanical engineering. From 2015 to 2018, he worked as a Software Engineer at Future Robot.

YOUNG-HA KWON received the B.S. degree in textile engineering from Kyung Hee University, Seoul, South Korea, and the M.S. and Ph.D. degrees in engineering mechanics from the University of Illinois at Chicago, USA, in 1982, 1984, and 1987, respectively. Since 1992, he has been with the Department of Mechanical Engineering, Kyung Hee University, Yongin, South Korea, where he is currently working as a Professor. His research interests include biomechanics, neuroscience, and sensors.